

DOI: 10.1002/ejic.201((will be filled in by the editorial staff))

Nerve Agent Degradation Using Polyoxoniobates

Mark K. Kinnan,^[a] William R. Creasy,^[b] Lauren B. Fullmer,^[c] Heidi L. Schreuder-Gibson,^[d]
May Nyman^{*[c]}

Keywords: polyoxometalate / polyoxoniobate / catalysis / ion-pairing / small-angle X-ray scattering / nerve agent

Polyoxoniobates are exceptional amongst polyoxometalates in that they can potentially perform base catalysis in water, a process in which a proton is bonded to an oxo ligand, and a hydroxyl is released. Catalytic decomposition of chemical warfare agents such as organofluorophosphates that were used recently in the infamous civilian attacks in Syria is one opportunity to employ this process. Upon evaluation of the polyoxoniobate Lindqvist ion, $[\text{Nb}_6\text{O}_{19}]^{8-}$, fast neutralization kinetics was discovered for the breakdown of the nerve agent simulant diisopropyl fluorophosphate (DFP). Further testing of the polyoxoniobates against nerve agents Sarin (GB), and Soman (GD) was also performed. It was determined that different Lindqvist counteranions (Li, K, or Cs)

affect the rate of decomposition of the organophosphate compounds in both aqueous media (homogeneous reaction), and in the solid-state (heterogeneous reaction). Small-angle X-ray scattering of solutions of the Li, K, and Cs $[\text{Nb}_6\text{O}_{19}]^{8-}$ salts at concentrations which the experiments were performed revealed distinct differences that could be linked to their relative reaction rates. This study represents the first demonstration of exploiting the unique alkaline reactivity of polyoxoniobates for nerve agent decontamination.

Introduction

Nerve agents are a type of organofluorophosphate (OP) compound that are used as Chemical Warfare Agents (CWAs). They release HF upon contact with moist skin or lungs and inhibit neural function; these were used in the recent infamous attacks on civilians in Syria.^[1] The deactivation and thus decontamination of nerve agents such as Sarin (GB) and Soman (GD) is accomplished via the cleavage of the phosphorus-fluorine bond in the molecule and replacement with a P-OH bond.^[2] Even though nerve agents auto-hydrolyze in water and high pH environments with time,^[3] decontaminating materials that can be attached to a surface while maintaining their reactive nature are of interest.^[4] This is particularly important for the development of fabrics or filtration media that can protect an individual from CWAs.^[4]

Over the years, a variety of different polymeric and inorganic materials have been evaluated for their ability to break down nerve agents and their simulants.^[5] When developing materials for decontamination applications the nerve agent simulant diisopropyl fluorophosphate (DFP) is typically employed due to its likeness to

GB and GD but lower toxicity. For polymeric materials, reactive moieties such as guanidine,^[6] hydroxamic acid,^[7] o-iodosylcarboxylate,^[8] and oxime^[9] groups have been demonstrated to be effective for the breakdown of nerve agents and/or their simulants. Inorganic materials such as metal chelates,^[10] TiO_2 ,^[11] $\text{Zr}(\text{OH})_4$,^[12] and polyoxometalates (POMs)^[13] have also been investigated. The advantage of POMs is the control they provide for surface functionalization. They are small and discrete, and can be dissolved in aqueous or nonaqueous solvent (depending on the counterion). This provides an easy and versatile mechanism for attaching them to a fabric or filtration media via electrostatics, or even covalent bond formation if they are appropriately functionalized. Furthermore, POMs are entirely inorganic, and thus robust and not subject to breakdown via exposure to environmental factors such as ultraviolet light.

In this paper, we strategically choose polyoxoniobates (PONbs) as reagents for the breakdown of DFP (diisopropyl fluorophosphate), GD (3,3-Dimethylbutan-2-yl methylphosphonofluoridate), and GB (Propan-2-yl methylphosphonofluoridate), see Figure 1, given their alkaline behavior. Although a variety of POMs such as transition-metal-substituted polyoxometalates,^[14] iron-substituted Keggin heteropolytungstate,^[15] and $\text{H}_5\text{PV}_2\text{Mo}_{10}\text{O}_{40}$ ^[16] have been tested for the breakdown of CWAs the focus has been on blister agents (e.g. mustard gas) which use different decomposition mechanisms that are not suitable for nerve agents. Blister agents are decontaminated via oxidation reactions whereas nerve agents are neutralized by base hydrolysis.

[a] Sandia National Laboratories, 1515 Eubank SE, Albuquerque, New Mexico 87123

[b] Leidos Corp, P.O. Box 68, Edgewood Chemical Biological Center, Aberdeen Proving Ground, Maryland 21010

[c] Oregon State University, Department of Chemistry, 153 Gilbert Hall, Corvallis, Oregon 97331-4003
Email: may.nyman@oregonstate.edu
Homepage: URL of homepage:
<http://chem.science.oregonstate.edu/nyman>

[d] U.S. Army Natick Soldier Research, Development & Engineering Center, 15 Kansas Street, Natick, Massachusetts 01760-5020

PONbs are the most basic of the known POMs due to their high charge density: they readily bind up to three protons in aqueous solution.^[17] With recent work, PONbs also exhibit size, geometry, composition and charge versatility, which can be exploited to tailor reactivity in base catalysis reactions.^[18] The Lindqvist ion, or hexaniobate, $[\text{Nb}_6\text{O}_{19}]^{8-}$ is the most studied PONb and its compact and highly symmetric geometry, consisting of six mutually edge-sharing octahedra forming a super-octahedron, is illustrated in Figure 1. The Lindqvist ion is highly stable and readily synthesized with all alkali counteranions and also tetramethylammonium, and thus is an ideal model system for this study.^[19] Moreover, this cluster has the highest charge-density of all POMs^[18], which directly correlates with its basicity. Both solid-state and solution^[17a] studies indicate that the μ_2 -bridging O^{2-} ligand is the favored protonation site over the doubly-bonded, terminal oxo ligand, and this is depicted in Figure 1.

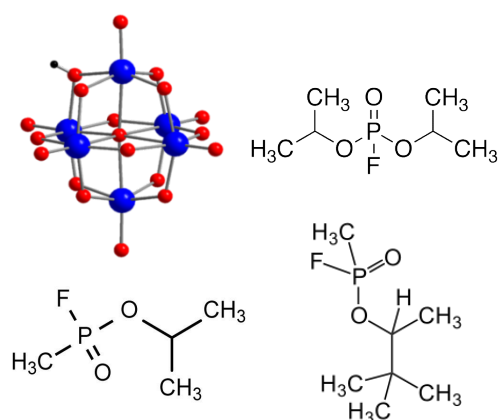


Figure 1. Schematics of: Top left: Ball and stick model of the Lindqvist ion $[\text{Nb}_6\text{O}_{19}]^{8-}$. Blue spheres are niobium; red spheres are oxygen. In this representation, two protonated μ_2 bridging oxo-ligand are shown (gray spheres). Top right: diisopropyl fluorophosphate (DFP) nerve agent simulant. Bottom left: nerve agent Sarin (GB), (*RS*)-Propan-2-yl methylphosphonofluoridate. Bottom right: nerve agent Soman (GD), 3,3-Dimethylbutan-2-yl methylphosphonofluoridate

The polyoxometalates of W, Mo, and V have been utilized in catalytic reactions quite extensively, as oxidation and acid catalysts in particular.^[20] On the other hand, catalytic reactivity studies of polyoxoniobates are rare. Heterogeneous photocatalysis has been recently demonstrated for PONbs, but requires the aid of co-catalysts.^[21] This current study represents the first demonstrated reaction of polyoxoniobates that can be carried out effectively both heterogeneously and homogeneously to exploit the unique alkaline reactivity of PONbs.

Results and Discussion

Nerve agents like GD and GB, as well as the simulant DFP are decomposed via cleavage of the phosphorus-fluorine bond to produce fluoride ion and a less toxic organophosphate compound.^[22] The decomposition of DFP via a bridging oxygen ligand in a Lindqvist ion is illustrated in Figure 2. The breakdown products of OP compounds can be conveniently measured in solution using a fluoride ion probe^[23] or by ^{31}P NMR^[2]. Solution based tests using OP compounds can be performed in minutes and

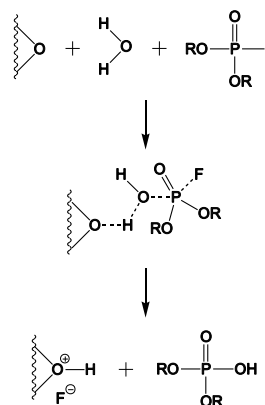


Figure 2. Illustration of the decomposition of diisopropyl fluorophosphate by the oxygen bridging ligand of the polyoxoniobate. R designates an isopropyl group.

are ideal for rapidly screening materials for potential decontamination activity. NMR, on the other hand, takes significantly longer to collect data but has the advantage of performing the reaction in a closed system by means of a capped NMR rotor. NMR can also simultaneously measure the OP compounds and breakdown products.

The kinetic data for the breakdown of OP compounds using PONbs is presented in Table 2 and also in Figure 3, a representative comparison of the activity of the $[\text{Nb}_6\text{O}_{19}]^{8-}$ Li, K and Cs salts. Upon solution based testing using the fluoride ion probe, fast neutralization kinetics was discovered for the breakdown of DFP, but the rate of DFP decomposition was significantly affected by the counteranion associated with the Lindqvist ion.

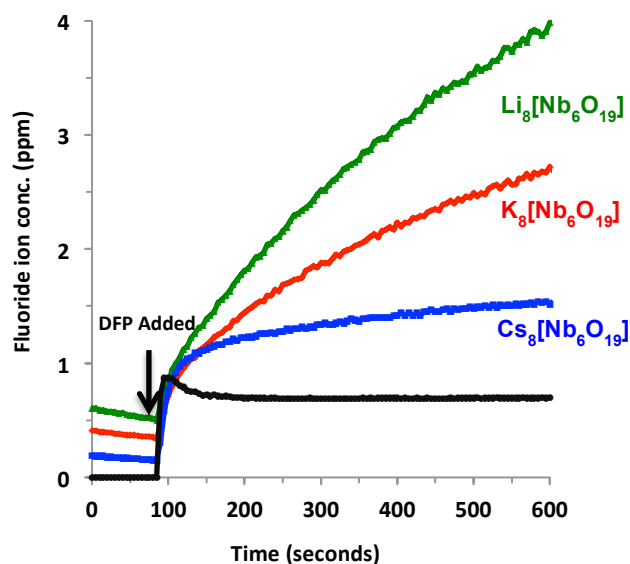


Figure 3. Comparing DFP decomposition rates, and the effect of the Li, K or Cs counterion. Reactions were performed in aqueous solutions with mole ratios of 3.6, 4.8, and 4.4 of DFP to the Li, K, and Cs PONb, respectively. A fluoride electrode was used to monitor the concentration of fluoride ion generated from the decomposition of DFP in solution.

Previously reported Small-Angle X-ray Scattering (SAXS) studies of the Lindqvist salts in solutions of 1-3 molar alkali hydroxide showed that contact ion-pairing of $[\text{Nb}_6\text{O}_{19}]^{8-}$ with Cs^+ dominates in aqueous media, whereas solvent-separated or solvent-shared ion-pairing of $[\text{Nb}_6\text{O}_{19}]^{8-}$ is the predominant state when K^+ is the counterion.^[24] The ion-association between Li^+ and the Lindqvist has not yet been probed, but based on the general trend of the alkalis it is assumed the Li^+ carries a large hydration sphere and is not closely associated with $[\text{Nb}_6\text{O}_{19}]^{8-}$. These prior studies are good controls for understanding cluster-counterion-association, in that the complicating effect of protonation of the clusters is eliminated. Here we perform SAXS analyses representative of the DFP neutralization studies presented in Figure 3. Figure 4a shows the scattering curves for 2mM solutions of Li^+ , K^+ and Cs^+ salts of $[\text{Nb}_6\text{O}_{19}]^{8-}$. Although the nerve agent neutralization reactions were performed with 1mM solutions of the Lindqvist salts, these solutions did not give enough scattering intensity to interpret accurately, so higher concentrations were necessary. There are distinct differences, and the form factors obtained from curve-fitting routines are summarized in Table 1. Additionally, the pair distance distribution function (PDDF) plots derived from the scattering curves are shown in Figure 4b.

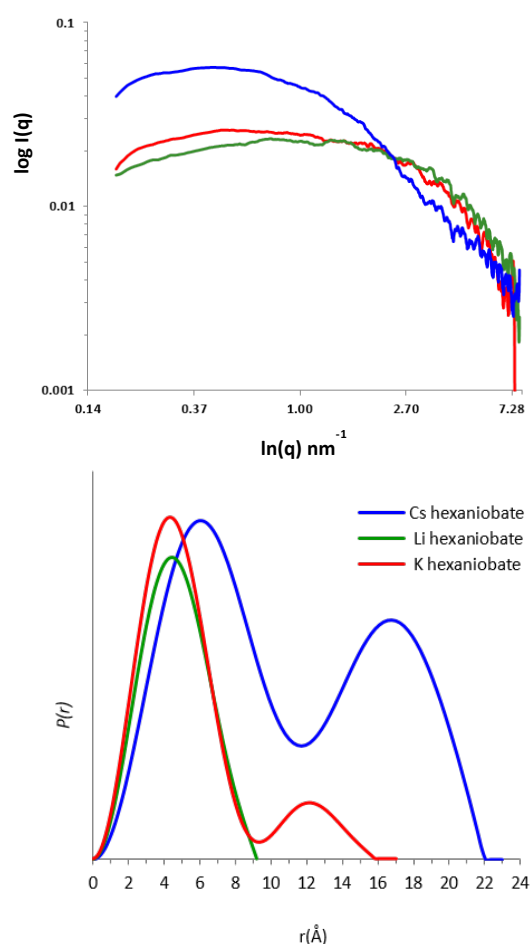


Figure 4. (top) X-ray scattering curves for 2mM $\text{Li}_8[\text{Nb}_6\text{O}_{19}]$, $\text{K}_8[\text{Nb}_6\text{O}_{19}]$ and $\text{Cs}_8[\text{Nb}_6\text{O}_{19}]$ dissolved in water. (bottom) Pair distance distribution function (PDDF) profiles from curve-fitting of the SAXS plots. Color scheme is the same for both plots, see legend in Figure 4b.

For $\text{Li}_8[\text{Nb}_6\text{O}_{19}]$, the radius of gyration (R_g , shape-independent parameter that describes the size of the scattering specie in

solution), associated radius ($\sim 1.29 \times R_g$ assuming a spherical particle), and PDDF profile all agree with a ‘nude’ $[\text{Nb}_6\text{O}_{19}]^{8-}$ anion that is not associated with any counterions (crystallographically determined radius of this specie is 4.2 Å). This is likely the reason why the $\text{Li}_8[\text{Nb}_6\text{O}_{19}]$ solution is most effective at catalyzing the neutralization of DFP in solution: its unassociated state allows direct contact with the DFP molecule. The 1mM $\text{Cs}_8[\text{Nb}_6\text{O}_{19}]$ solution clearly contains larger scattering species, as determined by the R_g , obtained by two methods (see Table 1). The PDDF profile of $\text{Cs}_8[\text{Nb}_6\text{O}_{19}]$ presents a classic curve of a dimerized primary scatterer in solution,^[25] as we have observed in prior SAXS studies of polyoxoniobates^[26]. The primary scatterer is considerably larger than the ‘nude’ Lindqvist ion, with a diameter of around 12 Å; and the long dimension of the dimer is approximately double, 22 Å. The 12 diameter is almost 4 Å bigger than the nude Lindqvist ion, and could indicate a shell of Cs^+ -cations directly bonded to the cluster. Two clusters of the dimer form could be associated by mutual H-bonding of the clusters’ protonated faces; as observed (and modeled from structural data as done prior,^[26] see SI). Without a solid-state model, we cannot describe the exact solution state of the Lindqvist ions, but a qualitative approximation is shown in the supplementary information. The $\text{Cs}_8[\text{Nb}_6\text{O}_{19}]$ solutions are not monodisperse as indicated by the shallow slope of the high- q region of the curve, which could not be reasonably fit (above $q=0.5 \text{ \AA}^{-1}$). Nonetheless, the curve-fitting routines indicate extensive clustering and ion-pairing. $\text{K}_8[\text{Nb}_6\text{O}_{19}]$ solutions like the $\text{Li}_8[\text{Nb}_6\text{O}_{19}]$ solutions consist primarily of the unassociated Lindqvist ions, but also contain a population of dimers (est. up to 30%), likely formed by mutual H-bonding of two diprotonated faces of the cluster without any associated K^+ . This is a motif we often observe in the solid-state,^[19c] and simulated^[27] SAXS data from solid-state structures. Simulated SAXS data are shown in the supplementary information for a monomeric Lindqvist ion, two Lindqvist ions dimerized by H-bonding, and linear combinations of pure monomer and pure dimer forms.

Table 1. SAXS analysis of Li, K and Cs $[\text{Nb}_6\text{O}_{19}]$ solutions; with and without DFP

Counterion	R_g from Guinier analysis ^[a]	Radius from Guinier R_g ^[b]	R_g from PDDF analysis ^[c]
2mM $[\text{Nb}_6\text{O}_{19}]$, without DFP			
Li^+	3.4 (4)	4.39	3.5 (1)
K^+	4.1 (2)	5.35	4.4 (2)
Cs^+	8.4 (2)	10.9	8.5 (2)
5mM $[\text{Nb}_6\text{O}_{19}]$, with DFP			
Li^+	3.0 (3)	3.87	3.08 (2)
K^+	3.3 (2)	4.26	3.31 (3)
Cs^+	3.7 (3)	4.77	3.76 (2)

^[a]between $q=0.18$ - 0.25 \AA^{-1} from $\ln(I)$ vs. q^2 plot

^[b]assuming approximate spherical radius; $R \sim 1.29 \times R_g$

^[c]PDDF=pair distance distribution function

We also analyzed via SAXS the solutions of the $[\text{Nb}_6\text{O}_{19}]$ salts containing the same concentration of DFP that was utilized in the degradation experiments. The scattering curves for these are shown in the SI, and the PDDF profiles are in figure 5. Initially, we obtained even weaker scattering curves from 2mM Lindqvist ion solutions with DFP; and thus we increased the $[\text{Nb}_6\text{O}_{19}]$ concentration to 5mM. Upon analysis of these data, the reason for the weaker scattering was self-evident: the scattering species were

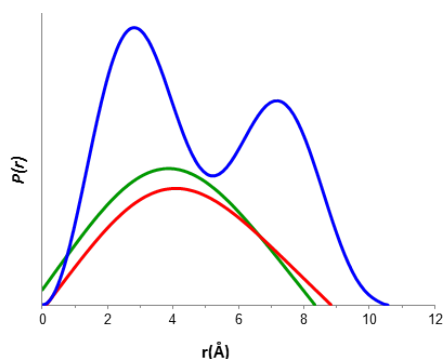


Figure 5. PDDF profiles for 5mM $\text{Li}_8[\text{Nb}_6\text{O}_{19}]$, $\text{K}_8[\text{Nb}_6\text{O}_{19}]$ and $\text{Cs}_8[\text{Nb}_6\text{O}_{19}]$ dissolved in water with DFP.

smaller in the presence of DFP, the Cs-analogue in particular (see Table 1). The scattering intensity decreases significantly with size of the scattering specie, since intensity is proportional to the sixth power of the radius. This alone was a significant observation, indicating that 1) the Lindqvist ions are not decomposing upon exposure to DFP or the HF byproduct; and 2) the DFP molecules partially disaggregate the alkali- $[\text{Nb}_6\text{O}_{19}]$ assemblies. If we add the DFP to the Lindqvist ion solution in great excess, we do indeed observe clouding and formation of very large particles via SAXS analysis. The PDDF profiles of the solutions containing DFP plus Li or K salts of $[\text{Nb}_6\text{O}_{19}]$ suggest mostly unassociated Lindqvist ion (see figure 5 and Table 1). The PDDF analysis of the DFP plus $\text{Cs}_8[\text{Nb}_6\text{O}_{19}]$ indicates that the dimerized state still dominates solution speciation. However, the linear extent and maxima of the curves (compared to the solutions without DFP) suggest that the Cs-counterions are less associated. These results collectively suggest that the DFP molecules do in fact displace associated alkalis, which would be important for the reaction with $[\text{Nb}_6\text{O}_{19}]$ to occur. Not entirely however, as the R_g -values determined by two methods (see Table 1) trend $\text{Li} < \text{K} < \text{Cs}$. As discussed earlier, the dimerization that occurs extensively for aqueous $\text{Cs}_8[\text{Nb}_6\text{O}_{19}]$, with and without DFP, is likely via mutual H-bonding of protonated faces. Thus we may hypothesize that these protonated faces are not

as accessible to DFP in the $\text{Cs}_8[\text{Nb}_6\text{O}_{19}]$ solutions, and the neutralization reaction is considerably hindered.

The association of clusters in solution by both ion-pairing with the counterions and H-bonding of protonated cluster faces increases with increasing counterion size $\text{Li} < \text{K} < \text{Cs}$. This leads to decreased availability for interacting with OP molecules and ultimately decreases efficacy of homogeneous reaction in water. The SAXS data also lends evidence for the mechanism of OP decomposition illustrated in Figure 2, where the transition state involves direct association of the protonated Lindqvist ion with the OP molecule rather than association of the OP molecule with a hydroxide generated via protonation of the Lindqvist cluster.

Further testing of the PONbs against DFP in a closed environment using significantly less water was performed in an NMR rotor monitored by ^{31}P solid-state NMR. This provided information on reactive behavior on a surface, which is closer to the state that would be employed for filtration media or protective clothing. The results revealed slower kinetics for $\text{Li}_8[\text{Nb}_6\text{O}_{19}]$ and $\text{K}_8[\text{Nb}_6\text{O}_{19}]$ compared to solution testing, but faster kinetics for $\text{Cs}_8[\text{Nb}_6\text{O}_{19}]$. Additionally, the observed decontamination rates were similar for each Lindqvist salt with no noticeable trend with respect to counterion. In the ^{31}P NMR experiment, the amount of water in the system is insufficient to provide complete dissolution of the Lindqvist salts resulting in a more heterogeneous system. These reactions contained a Lindqvist salt and a small quantity of water creating a saturated solution of Lindqvist salt and undissolved PONb. Figure 6 shows a representative ^{31}P NMR spectra of the breakdown of DFP to diisopropyl phosphate (DIPP) for a heterogeneous solution. For the specific case of $\text{Cs}_8[\text{Nb}_6\text{O}_{19}]$, k_{obs} and $t_{1/2}$ are slower for solution testing than NMR testing. With solution testing, there is the additional element of OP molecule diffusion to the molecule followed by interaction with the Lindqvist ion. This effect in conjunction with the close association of Cs^+ to Lindqvist ion hinders decontamination at high volumes of water. For small volumes of water, diffusion of the OP molecule is a less important factor.

Table 2. Kinetic data for the breakdown of organophosphate (OP) compounds using polyoxoniobates (PONbs).

Material	OP	Measurement (type)	Mole Ratio (OP:PONb)	RXN Volume (mL)	k_{obs} (s^{-1})	$t_{1/2}$ (h)
$\text{Li}_8\text{Nb}_6\text{O}_{19}$	DFP ^[a]	Ion Probe	3.6 ± 0.3	10.	$6.0 \times 10^{-5} \pm 0.8 \times 10^{-5}$	3.2 ± 0.4
$\text{K}_8\text{Nb}_6\text{O}_{19}$	DFP	Ion Probe	4.8 ± 0.5	10.	$3.4 \times 10^{-5} \pm 0.3 \times 10^{-5}$	5.7 ± 0.4
$\text{Cs}_8\text{Nb}_6\text{O}_{19}$	DFP	Ion Probe	4.4 ± 0.2	10.	$8.3 \times 10^{-6} \pm 3 \times 10^{-6}$	27 ± 13
$\text{Li}_8\text{Nb}_6\text{O}_{19}$	DFP	NMR	2.8	0.11	1.86×10^{-5}	10.38
$\text{K}_8\text{Nb}_6\text{O}_{19}$	DFP	NMR	2.1	0.11	1.92×10^{-5}	10.04
$\text{Cs}_8\text{Nb}_6\text{O}_{19}$	DFP	NMR	2.5	0.12	1.80×10^{-5}	10.69
$\text{Li}_8\text{Nb}_6\text{O}_{19}$	GD ^[b]	NMR	0.50	0.22	7.04×10^{-4}	0.27
$\text{Li}_8\text{Nb}_6\text{O}_{19}$	GD	NMR	5.55	0.23	3.93×10^{-4}	0.50
$\text{Li}_8\text{Nb}_6\text{O}_{19}$	GD	NMR	22.18	0.23	1.25×10^{-4}	$> 1.54^{[d]}$
$\text{Li}_8\text{Nb}_6\text{O}_{19}$	GB ^[c]	NMR	0.97	0.66	6.0×10^{-3}	0.03
$\text{K}_8\text{Nb}_6\text{O}_{19}$	GB	NMR	1.62	0.11	5.7×10^{-3}	0.03
$\text{Cs}_8\text{Nb}_6\text{O}_{19}$	GB	NMR	1.56	0.12	5.5×10^{-3}	0.04

^[a] diisopropyl fluorophosphate

^[b] 3,3-Dimethylbutan-2-yl methylphosphonofluoridate

^[c] Propan-2-yl methylphosphonofluoridate

^[d] Rate constant is shown for the first 0.5 hr, but the rate slows down after 0.5 hr. See text for discussion.

Following testing of DFP with the three Lindqvist salts, additional breakdown testing was performed using GD and GB at Edgewood Chemical Biological Center, see Table 2 and SI5 and SI6. GD was only tested utilizing $\text{Li}_8[\text{Nb}_6\text{O}_{19}]$. In this case, the mole ratio of GD to PONb was different for each test to determine any effects on the kinetics. It was observed that as the mole ratio of GD:PONb. increased, k_{obs} decreased and the half-life increased. The results from those tests revealed a range in GD half-life from 0.27 to >1.54 hr, almost an order of magnitude, for a mole ratio from 0.5 to 22 for GD:LiPONb. For the mole ratio of 22, the pseudo-first order kinetic plot was not linear and showed a marked decrease in rate after 0.5 hr. The kinetic plots are shown in the Supporting Information. The reason for the rate change is not clear and requires more research. One possibility is that at lower concentrations of GD in solution, the diffusion of GD molecules to an active site on a Lindqvist ion is likely the rate-limiting step. By increasing the concentration of GD, the time for diffusion of a GD molecule to a Lindqvist ion decreases. At higher mole ratios there is a higher rate of interaction between the GD molecules and the Lindqvist ion. Another possible explanation is that there is a pH change from the degradation of GD, since the degradation produces acid products, which can result in more protonation of the Lindqvist ions, and therefore higher reactivity. However, excessive protonation eventually results in decomposition of the Lindqvist ions. These results illustrate the importance of evaluating decontamination materials at several different mole ratios.

Tests with DFP and GB were performed using similar quantities of PONb and agent. The GB reaction kinetics were extremely fast with half-lives on the order of minutes. Since the chemical structures of GB and GD are similar, one would expect the kinetic breakdown rates to be similar. However, GB has a higher water solubility^[28] than GD yielding faster diffusion of the GD molecules to the Lindqvist ions. As observed with DFP, the Li^+

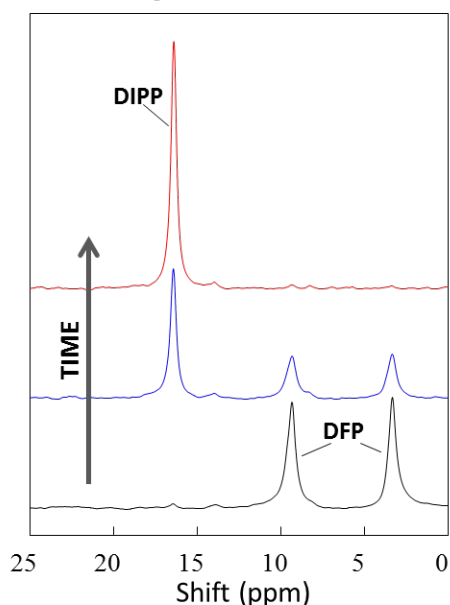


Figure 6. A representative ^{31}P NMR spectra of the breakdown of diisopropyl fluorophosphate (DFP) to diisopropyl phosphate (DIPP) for a heterogenous solution. The DFP peak is split via ^{19}F - ^{31}P ^1J -coupling.

Lindqvist salt exhibited the fastest kinetics; an order of magnitude faster than the Lindqvist salts of K^+ and Cs^+ , again indicating the importance of counterion association. After reaction,

^{19}F NMR was used to determine whether any new fluorine containing compounds were formed, but no new ^{19}F peaks were observed.

Comparing the kinetic data reported in this manuscript to kinetic data from other neutralization materials in the literature is difficult. There are many studies of different materials for neutralization of a variety of CWAs and simulants. Challenges associated with comparing data to prior reported studies include: (1) differences in analytical techniques, (2) differences in CWAs and/or simulants, (3) different molar ratios of CWA and/or simulant to the neutralization catalyst. In particular, many previous studies have used much lower ratios of CWA to decontamination agent. In some prior studies, a liquid phase reaction was mixed or agitated to allow a larger amount of decontaminant to come into contact with the OP. For example, one report used polyacrylamidoxime (PANOX)^[29] for the neutralization of GD. The kinetic observations for k_{obs} and $t_{1/2}$ are $3.6 \times 10^{-4} \text{ s}^{-1}$ and 0.54 hours, respectively. Another example is the breakdown of GD using $\text{Zr}(\text{OH})_4$ ^[12] in which $t_{1/2}$ is reported to be 0.15 hours. In both of these examples, the approximate calculated mole ratio of GD to neutralization catalyst ranged from approximately 0.01 to 0.02. In contrast, the results in Table 2 for GD neutralization using $\text{Li}_8[\text{Nb}_6\text{O}_{19}]$ were obtained with mole ratios of up to 22.

Conclusions and Future Directions

The alkaline nature of polyoxoniobates renders them unique amongst polyoxometalates, and this characteristic has yet to be exploited in practical applications. Reported in this paper is the first demonstration of the use of polyoxoniobate Lindqvist ions, $[\text{Nb}_6\text{O}_{19}]^{8-}$, for the breakdown of the CWAs GD, and GB and the CWA simulant DFP. Due to the basic behavior of these PONbs, they are most effective for this base-catalyzed reaction. On the other hand, prior studies showed blister agents could be neutralized by redox active POMs^[14]. In combination, these two types of chemically unique POMs could potentially provide the complete package for providing protective clothing or filtration against chemical warfare agents. Even more intriguing is the very recent developments of incorporating redox active transition-metals into the alkaline POMs^[30], which may provide opportunity for a POM cluster that could function in both redox active reactions and base catalysis.

Our next steps in this work include functionalizing surfaces with the alkaline PONbs and testing their surface reactivity toward CWA decontamination. These studies will also involve fundamental investigation of mechanisms of POM attachment to the surface. New CWA decontamination systems are becoming specialized to address specific applications. Although a fast decontamination reaction rate is important, materials with properties that fit the application are more critical. We will exploit the high anionic charge of the PONb to electrostatically bind it to fabric treated with cationic ammonium terminal groups. Recent studies by Weinstock indicate the counterions may play a significant role in the POM attachment mechanism.^[31] Therefore, POM-surface functionalization studies will also provide insight into the role of counterions in base catalysis reactivity, as was distinctly observed in the solution studies reported here.

Experimental Section

Materials. Lithium hydroxide, potassium hydroxide, cesium hydroxide, and diisopropyl fluorophosphate were purchased from Sigma-Aldrich. *Hazard: Diisopropyl fluorophosphate is an extremely toxic chemical and should be handled appropriately.* Hydrous niobium oxide was acquired from Reference Metals Company Inc. All chemicals were used as received. Water with a resistivity greater than 18 MΩ•cm was used for all solutions.

PONb Synthesis. The synthesis of lithium, potassium and cesium Lindqvist salts from hydrous niobium oxide and respective alkali hydroxides has been described prior.^[19a, 19c] Following synthesis, the Lindqvist salts were recrystallized by dissolving in a minimal amount of water and precipitating by rapid addition of methanol. This process is repeated three times to remove excess free base to ensure the base-hydrolysis is occurring via the Lindqvist ion rather than a hydroxide contaminant. Characterization to determine protonation state, identification of phase, and number of water molecules per formula unit was carried out by powder X-Ray diffraction and thermogravimetry.

Small-angle X-ray scattering data were collected on an Anton Paar SAXSess instrument utilizing Cu-Kα radiation (1.54 Å) and line collimation. Solutions containing 2 or 5 mMolar Lindqvist salt, with or without DPF, were sealed in a 1.5 mm diameter glass capillary tube for SAXS measurements and measured for 2 hrs each. Background solutions were measured likewise. SAXSquant software was used for data collection and treatment (normalization, primary beam removal, background subtraction, desmearing, and smoothing to remove extra noise created by the desmearing routine). R_g (radius of gyration in the Guinier region of the scattering curve) was also determined utilizing SAXSquant. All other analyses and fits to determine size, shape, size distribution and PDDF (pair distance distribution function) were carried out utilizing the IRENA macros within IgorPro 6 (Wavemetrics) software.^[32]

Solution Ion Probe Studies of DFP (NSRDEC). An Orion Dual Star pH/ISE Benchtop Meter equipped with an Orion 9409BN fluoride electrode was used to monitor the concentration of fluoride ion generated from the decomposition of diisopropyl fluorophosphate in solution.^[23] An example of an experiment run is as follows. An amount of PONb equivalent to 8.0×10^{-6} moles was weighed out in a glass petri dish. 9.0mL of water was added to the petri dish followed by the addition of a stir bar to mix the solution. The first 90 seconds of the run was to establish equilibrium between PONb dissolved in water and the fluoride ion probe. At 90 seconds, 1.0 mL of DFP solution (DFP in water) was added to the petri dish. Data was logged on a computer connected to the Orion Dual Star Meter via a USB cable. The fluoride ion concentration was measured in parts per million every 5 seconds. Average data for ion probe testing in Table 1 was calculated from triplicate runs.

Solid-State NMR Studies of DFP (NSRDEC). The use of solid-state NMR to monitor OP decontamination has been described in detail previously.^[2] A weighed quantity of PONb equivalent to 1.0×10^{-5} moles was added to a 4 mm Bruker MAS zirconia rotor (Art. Nr.: B5679) followed by the addition of 4 μL of DFP. A 100 μL aliquot of water was then added to solvate the PONb and the rotor capped using Kel-F Drive Caps (4mm) (Art. Nr.: B5677). The degradation of DFP was monitored using a Bruker Avance 400 spectrometer, operating at 161.92 MHz (³¹P). The High Resolution Magic Angle Spinning (HR) MAS spectra were recorded with a 4 mm Bruker ³¹P HR MAS standard bore gradient probe (BL4HPCD) at ambient temperature (18 °C) using a phosphorous observed single pulse experiment with the magic-angle spinning rate of 5000 Hz. The following parameters were applied: center frequency of the acquisition (O1P), -16 ppm; sweep width, 62.7 ppm; number of scans, 100; excite pulse length (pw90), 8 μs; relaxation delay, 2 s; total experiment run time,

6.2 min. For the kinetic determinations, it was necessary to trade off precision with acquisition speed for fast data collection. The HR MAS spectra were externally calibrated (zeroed) to the one peak of triphenyl phosphate (-17.8 ppm, depending on solvent, relative to phosphoric acid standard).

NMR Studies of GD and GB (ECBC). Initial experiments were performed using a Bruker Avance 500 spectrometer to reproduce the conditions used at Natick. The instrument operated at 202.46 MHz (³¹P). The HRMAS spectra were recorded with a 5-mm Bruker ³¹P gradient probe at ambient temperature (23 °C) using a 1-D proton decoupled decay experiment with the magic-angle spinning rate of 5000 Hz. The following parameters were applied: center frequency of the acquisition (O1P), 20 ppm (4049 Hz); sweep width, 200.8 ppm; number of scans, 128; excite pulse length (pw90), 8 μs; recycle delay, 3 s; total experiment run time, 7.5 min. Small relative distortions of the relative peak areas, due to the short recycle delay, were about the same as or less than the spectral signal-to-noise ratios. For the kinetic determinations, it was necessary to trade off precision with acquisition speed to obtain fast data acquisition.

Due to limited availability of the Bruker Avance 500, comparison studies were done on a Bruker 300 NMR with a liquids probe. It was observed that the water added to the sample was sufficient to dissolve the PONb; therefore, a solids NMR probe was not needed since the agent was not spiked on a solid matrix. However, it was necessary to add extra water (220 μl instead of 100 μl) to fill the 5 mm NMR tube to the detection coil of the liquids probe. The extra water affected the molar concentration of the solution. Also, 10% D₂O was added as a lock solvent, and no studies were done to determine whether it affected the kinetics.

Kinetics of OP Neutralization. Calculating the kinetic data as it relates to decontamination has been described in detail previously and will only be briefly outlined.^[5, 29, 33] The time-dependent degree of conversion, F_t , of agent to breakdown product(s) was calculated using:

$$F_t = \frac{\sum I_p}{\sum I_a + \sum I_p}$$

where $\sum I_p$ and $\sum I_a$ are the sum of the integration of signals for breakdown product(s) and agent, respectively. The observed rate (k_{obs}) can then be calculated on the assumption of a pseudo first-order rate equation:

$$\ln(1 - F_t) = -k_{obs}t$$

followed by the calculation of half-life by:

$$t_{1/2} = \frac{\ln(2)}{k_{obs}}$$

Acknowledgments

LF and MN acknowledge Oregon State University for support on collection and interpretation of SAXS data. MK acknowledges Sandia National Laboratories internal funding for support. Sandia is a multiprogram laboratory operated by Sandia Corporation, a Lockheed Martin Company, for the United States Department of Energy under Contract DE-AC04-94AL85000. Additional funding was provided by the Defense Threat Reduction Agency for live agent testing at ECBC by Science Applications International Corporation (SAIC) under contracts DAAD13-03-D-0017 and W911SR-11-C-0047. This article has been reviewed and approved for public release: SAND-2013-1728 J and PAO U13-083.

- [1] a) M. B. D. Nikitin, P. K. Kerr, A. Feickert, Syria's Chemical Weapons: Issues for Congress, 2013, report # R42848 ; b) Organization for the Prohibition of Chemical Weapons, United Nations Mission to Investigate Allegations of the Use of Chemical Weapons in the Syrian Arab Republic,
- [2] G. W. Wagner, P. W. Bartram, *J. Mol. Catal. A-Chem.* **1999**, *144*, 419-424.

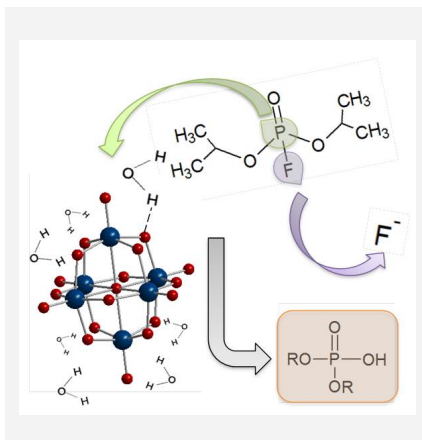
- [3] G. Lunn, E. B. Sansone, *Appl. Biochem. Biotechnol.* **1994**, *49*, 165-172.
- [4] H. L. Schreuder-Gibson, Q. Truong, J. E. Walker, J. R. Owens, J. D. Wander, W. E. Jones, *MRS Bull.* **2003**, *28*, 574-578.
- [5] Y. C. Yang, J. A. Baker, J. R. Ward, *Chemical Reviews* **1992**, *92*, 1729-1743.
- [6] L. Bromberg, T. A. Hatton, *Polymer* **2007**, *48*, 7490-7498.
- [7] L. Chen, L. Bromberg, J. A. Lee, H. Zhang, H. Schreuder-Gibson, P. Gibson, J. Walker, P. T. Hammond, T. A. Hatton, G. C. Rutledge, *Chem Mater* **2010**, *22*, 1429-1436.
- [8] a) L. Bromberg, H. Zhang, T. A. Hatton, *Chem Mater* **2008**, *20*, 2001-2008; b) H. Morales-Rojas, R. A. Moss, *Chemical Reviews* **2002**, *102*, 2497-2522.
- [9] L. Bromberg, T. A. Hatton, *Ind. Eng. Chem. Res.* **2007**, *46*, 3296-3303.
- [10] a) Y. W. Xie, B. N. Popov, *Anal. Chem.* **2000**, *72*, 2075-2079; b) Y. W. Xie, B. N. Popov, *Anal. Chim. Acta* **2001**, *448*, 221-230.
- [11] A. Kiselev, A. Mattson, M. Andersson, A. E. C. Palmqvist, L. Osterlund, *J. Photochem. Photobiol. A-Chem.* **2006**, *184*, 125-134.
- [12] T. J. Bandoz, M. Laskoski, J. Mahle, G. Mogilevsky, G. W. Peterson, J. A. Rossin, G. W. Wagner, *J. Phys. Chem. C* **2012**, *116*, 11606-11614.
- [13] a) F.-J. Ma, S.-X. Liu, C.-Y. Sun, D.-D. Liang, G.-J. Ren, F. Wei, Y.-G. Chen, Z.-M. Su, *J Am Chem Soc* **2011**, *133*, 4178-4181; b) D. M. Mizrahi, S. Saphier, I. Columbus, *J. Hazard. Mater.* **2010**, *179*, 495-499.
- [14] C. L. Hill, N. M. Okun, D. A. Hillesheim, Y. V. Geletii, in *Antiterrorism and Homeland Defense: Polymers and Materials, Vol. 980* (Eds.: J. G. Reynolds, G. E. Lawson, C. J. Koester), Amer Chemical Soc, Washington, **2007**, pp. 198-209.
- [15] a) N. M. Okun, T. M. Anderson, C. L. Hill, *J Am Chem Soc* **2003**, *125*, 3194-3195; b) N. M. Okun, J. C. Tarr, D. A. Hilleshiem, L. Zhang, K. I. Hardcastle, C. L. Hill, *Journal of Molecular Catalysis A: Chemical* **2006**, *246*, 11-17.
- [16] R. D. Gall, C. L. Hill, J. E. Walker, *Chem Mater* **1996**, *8*, 2523-2527.
- [17] a) J. R. Black, M. Nyman, W. H. Casey, *J Am Chem Soc* **2006**, *128*, 14712-14720; b) T. M. Alam, M. Nyman, B. R. Cherry, J. M. Segall, L. E. Lybarger, *J Am Chem Soc* **2004**, *126*, 5610-5620.
- [18] M. Nyman, *Dalton Transac* **2011**, *40*, 8049-8058.
- [19] a) T. M. Anderson, S. G. Thoma, F. Bonhomme, M. A. Rodriguez, H. Park, J. B. Parise, T. M. Alam, J. P. Larentzos, M. Nyman, *Cryst. Growth Des.* **2007**, *7*, 719-723; b) C. A. Ohlin, E. M. Villa, W. H. Casey, *Inorg. Chim. Acta* **2009**, *362*, 1391-1392; c) M. Nyman, T. M. Alam, F. Bonhomme, M. A. Rodriguez, C. S. Frazer, M. E. Welk, *J Clust Sci* **2006**, *17*, 197-219.
- [20] T. Okuhara, N. Mizuno, M. Misono, *Appl. Catal. A-Gen.* **2001**, *222*, 63-77.
- [21] a) Z. Y. Zhang, Q. P. Lin, D. Kurunthu, T. Wu, F. Zuo, S. T. Zheng, C. J. Bardeen, X. H. Bu, P. Y. Feng, *J Am Chem Soc* **2011**, *133*, 6934-6937; b) Z. L. Wang, H. Q. Tan, W. L. Chen, Y. G. Li, E. B. Wang, *Dalton Transac* **2012**, *41*, 9882-9884.
- [22] N. B. Munro, S. S. Talmage, G. D. Griffin, L. C. Waters, A. P. Watson, J. F. King, V. Hauschild, *Environ. Health Perspect.* **1999**, *107*, 933-974.
- [23] F. C. Hoskin, J. E. Walker, C. M. Mello, *Chemico-biological interactions* **1999**, *119-120*, 399-404.
- [24] M. R. Antonio, M. Nyman, T. M. Anderson, *Angew Chem Int Edit* **2009**, *48*, 6136-6140.
- [25] C. D. Putnam, M. Hammel, G. L. Hura, J. A. Tainer, *Q Rev Biophys* **2007**, *40*, 191-285.
- [26] Y. Hou, L. N. Zakharov, M. Nyman, *J Am Chem Soc* **2013**, *135*, 16651-16657.
- [27] D. M. Tiede, R. T. Zhang, L. X. Chen, L. H. Yu, J. S. Lindsey, *J Am Chem Soc* **2004**, *126*, 14054-14062.
- [28] Potential Military Chemical/ Biological Agents and Compounds FM 3-11.9, MCRP 3-37.1B, NTRP 3-11.32, and AFTTP(I) 3-2.55, Jan 2005, report
- [29] L. Bromberg, H. Schreuder-Gibson, W. R. Creasy, D. J. McGarvey, R. A. Fry, T. A. Hatton, *Ind. Eng. Chem. Res.* **2009**, *48*, 1650-1659.
- [30] a) J. H. Son, C. A. Ohlin, R. L. Johnson, P. Yu, W. H. Casey, *Chem-Eur J* **2013**, *19*, 5191-5197; b) J. H. Son, C. A. Ohlin, E. C. Larson, P. Yu, W. H. Casey, *Eur J Inorg Chem* **2013**, 1748-1753; c) J.-H. Son, C. A. Ohlin, W. H. Casey, *Dalton Transac* **2012**, *41*, 12674-12677.
- [31] Y. F. Wang, I. A. Weinstock, *Chem Soc Rev* **2012**, *41*, 7479-7496.
- [32] J. Ilavsky, P. R. Jemian, *J Appl Crystallogr* **2009**, *42*, 347-353.
- [33] D. Waysbort, D. J. McGarvey, W. R. Creasy, K. M. Morrissey, D. M. Hendrickson, H. D. Durst, *J. Hazard. Mater.* **2009**, *161*, 1114-1121.

Received: ((will be filled in by the editorial staff))
Published online: ((will be filled in by the editorial staff))

Layout 1:

Key Topic

Polyoxometalates, like small pieces of metal oxide, can be dissolved or fixed on a surface to respectively perform homogenous or heterogeneous catalysis. Here we exploit the alkaline nature of polyoxoniobates to neutralize nerve agents in both solution and the solid-state. Solution studies correlate reaction efficacy to the association of the dissolved polyoxoniobate with its counterions.



**Mark K. Kinnan, William R. Creasy,
 Lauren B. Fullmer, Heidi L.
 Schreuder-Gibson, May Nyman***
 Page No. – Page No.

Nerve Agent Degradation using
 Polyoxoniobates

Keywords: polyoxometalate /
 polyoxoniobate / catalysis / ion-pairing /
 small-angle X-ray scattering / nerve
 agent

Supporting Information

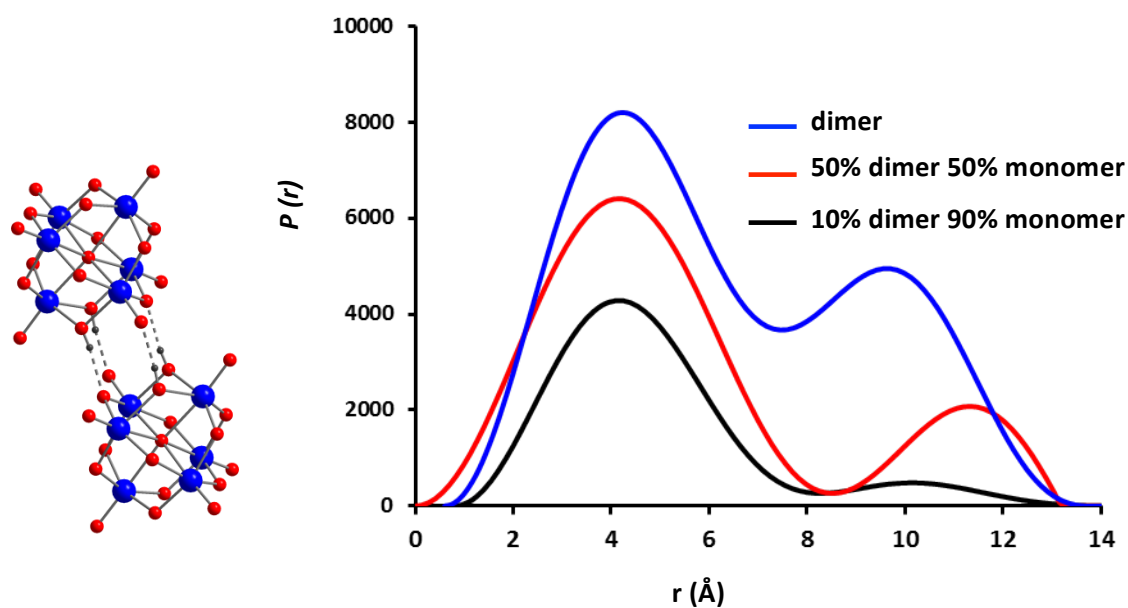


Figure SI1. Left: An H-bonded dimer of $[\text{H}_2\text{Nb}_6\text{O}_{19}]^{6-}$, as is frequently observed in the solid-state.^[19c] Blue spheres are Nb, red spheres are O, black spheres are H. The H-bonds, indicated by the broken lines are strong, with an H---O distance of 1.8-1.9 Å. Right: simulated PDDF's of mixtures of monomers and H-bonded dimers for qualitative comparison to $\text{K}_8[\text{Nb}_6\text{O}_{19}]$ solution.

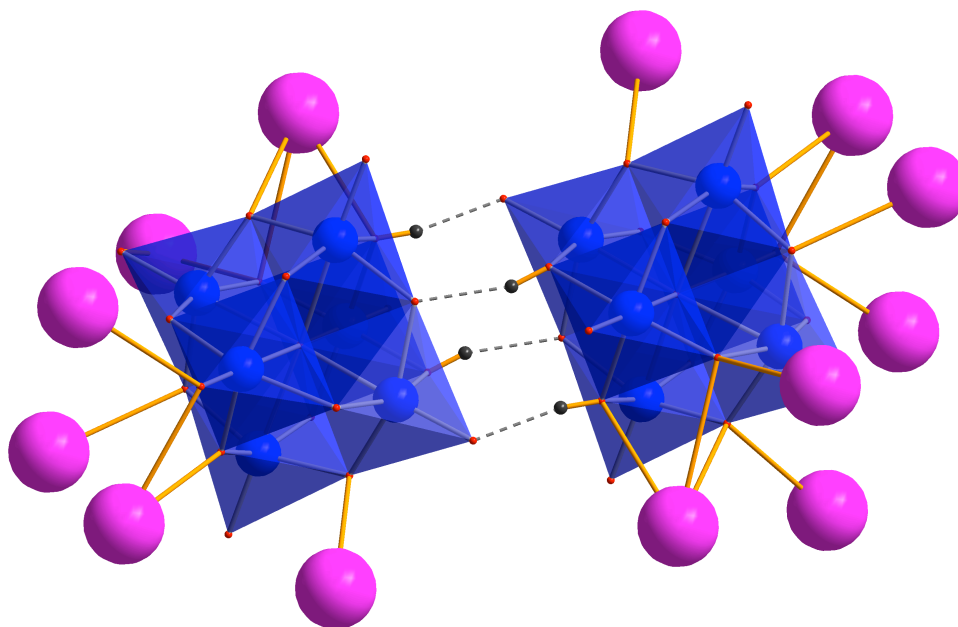


Figure SI2. A possible model for the primary scattering specie of 2 mM $\text{Cs}_8[\text{Nb}_6\text{O}_{19}]$ solution.

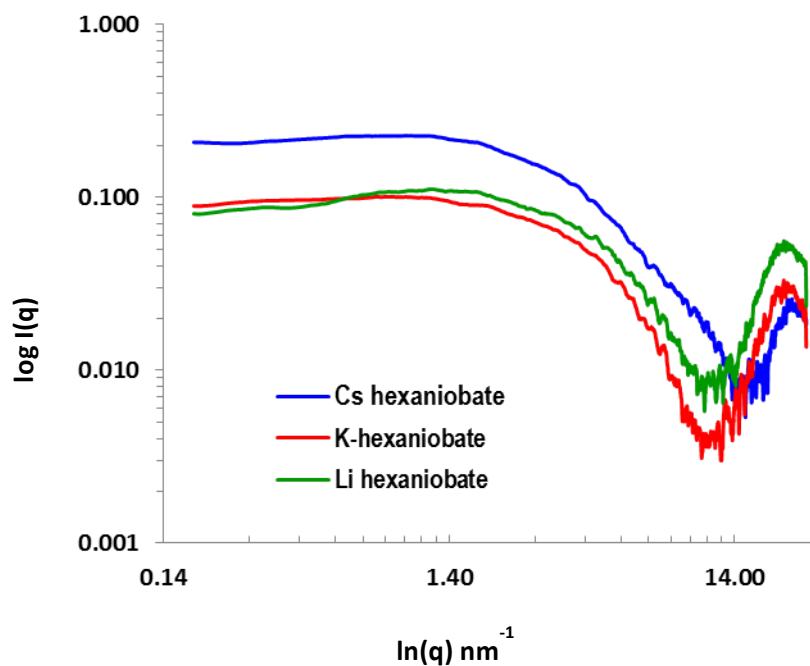


Figure SI3. X-ray scattering curves for 5mM $\text{Li}_8[\text{Nb}_6\text{O}_{19}]$, $\text{K}_8[\text{Nb}_6\text{O}_{19}]$ and $\text{Cs}_8[\text{Nb}_6\text{O}_{19}]$ dissolved in water with DFP added.

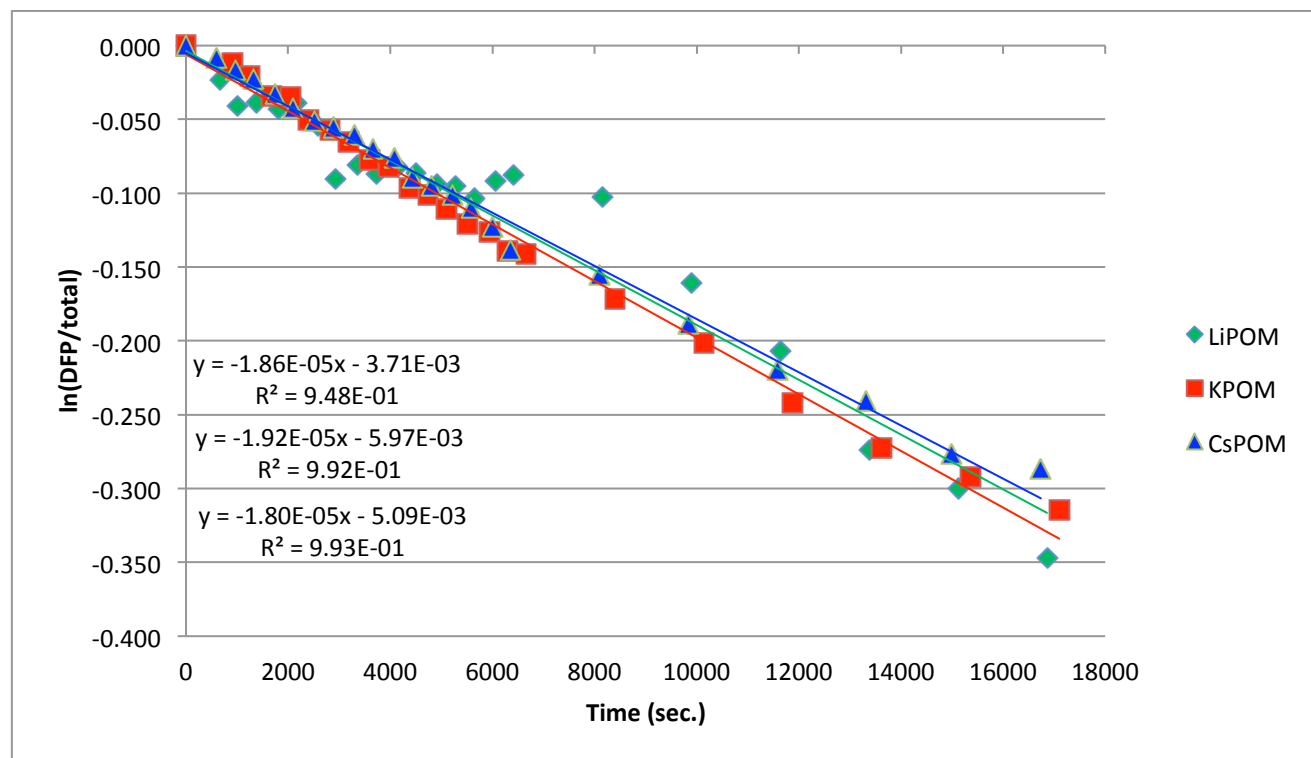


Figure SI4. Kinetic plot of the reaction of DFP with LiPOM (mole ratio 2.8), KPOM (mole ratio 2.1), and CsPOM (mole ratio 2.5).

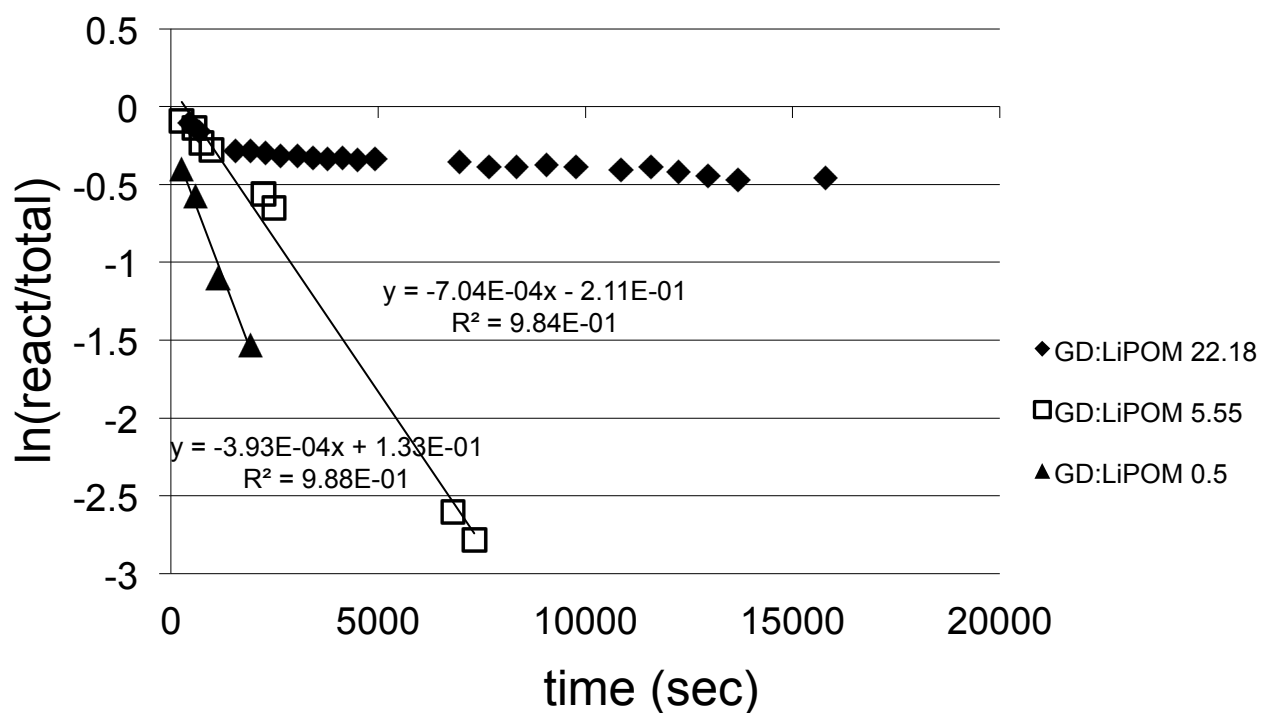


Figure SI5. Kinetic plot of the reaction of GD with LiPOM at mole ratios GD:LiPOM of 22.18, 5.55, and 0.5. Best fit lines are shown for the last two.

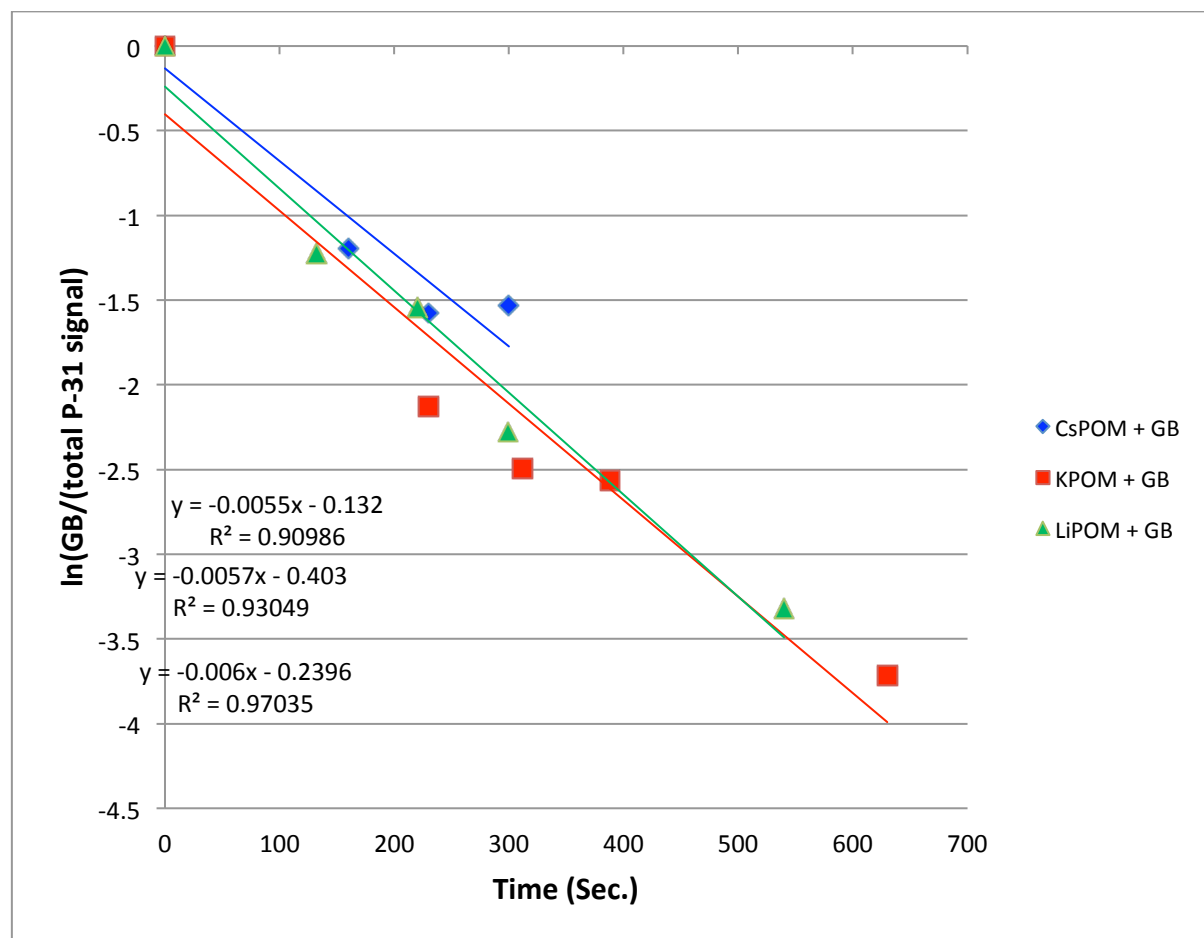


Figure SI6. Kinetic plot of the reaction of GB with LiPOM (mole ratio 0.97), KPOM (mole ratio 1.62), and CsPOM (mole ratio 1.56).